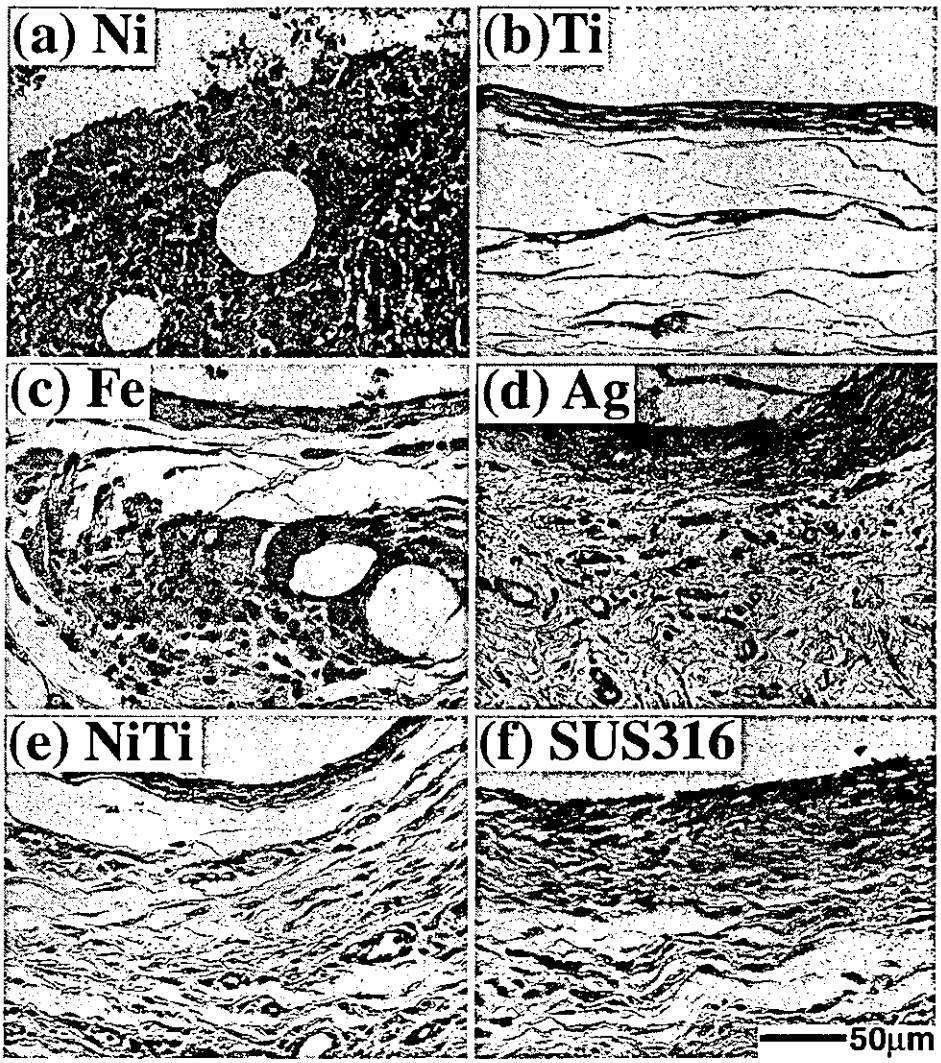

Fig. 9. Tissue reaction to Ni (a), Ti (b), Fe (c), Ag (d), NiTi (e) and SUS316 (e) after 1 week implantation in rat.

particles work more effectively to decompose HAP in vaccum and make dephosphoration. This leads to the formation of $CaTiO_3$ where P is not included as component, which explains well the XSAM mapping of Fig. 3.

Brinell hardness changed inside the Ti/HAP FGM in Fig. 4 showed that the hardness was low in the center region where Ti and HAP were mixed with comparable content (Fig. 5a). This is partly due to the decrease of compressing effect in the center of compact, remote from surface, by friction between particles in the CIP compacting process [25]. Another reason may be due to the decomposition occurred in the mixed region of Ti and HAP, since more than 1150 °C is necessary for sintering of Ti and HAP in the electric furnace method. The delayed expansion occurred and lead to autodestruction approximately in a month after fabrication due to the decomposition of HAP and the residual stress. To prevent this phenomenon, improvements in both materials and methods have been done.

Although the same phenomena occurred in SPS method, we could successfully prepare the Ti/HAP FGM by removal of Ti finer particles smaller than 1 μm using the sedimentation method for elimination and by lowering the sintering temperature to 850 °C.

4.1.1. Starting materials

HAP as prepared by wet methods are deviated from stoichiometry and generally unstable under heat treatments. HAP sintered at more than 1150 °C in air shows the peak due to stretching mode of OH.. group in FT-IR and Raman spectroscopy [18], which does not appear or is very small in HAP as prepared in wet method. Sintered HAP is close to stoichiometric and more stable to heat treatment. The HAP frit prepared by pulferization after sintered was used as starting material for HAP.

For Ti the particles of Ti hydrate instead of pure Ti seemed more favorable for sintering. Ti fine particles less than 1 μm causes more decomposition of HAP. The

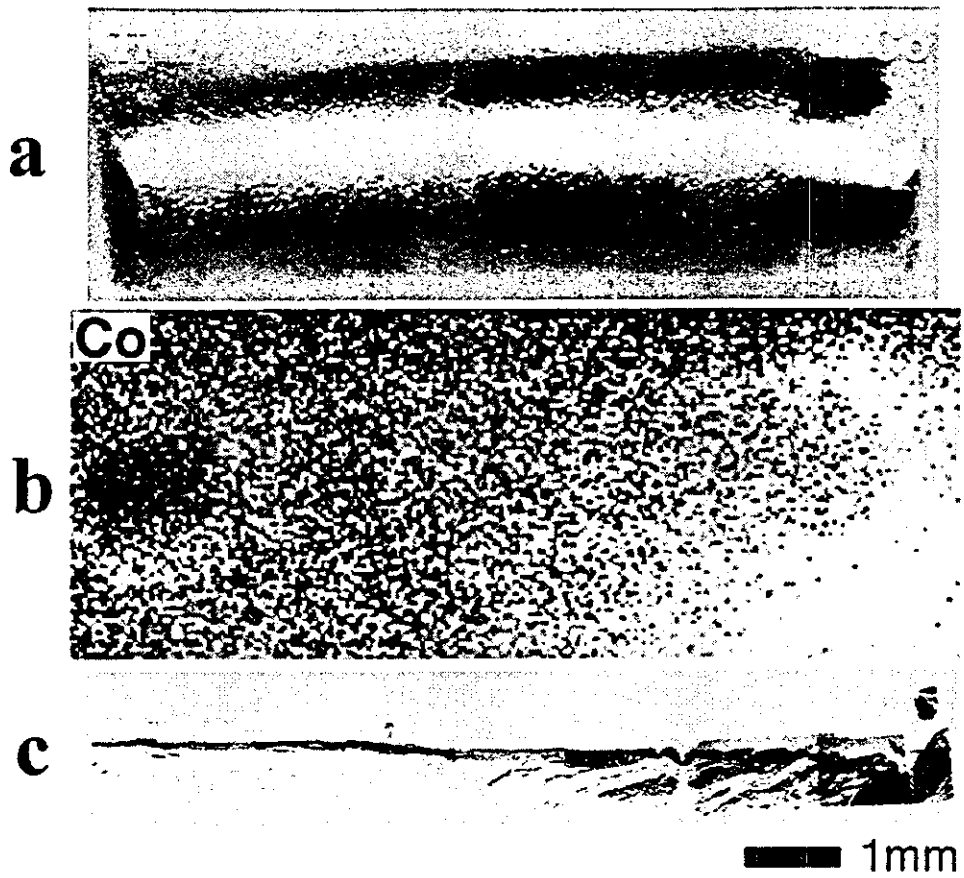

Fig. 10. Correlation of Ti/Co FGM (a), dissolution area of Co (b) and surrounding tissue reaction (c) after 2 week implantation in subcutaneous tissue of rat.

325 mesh pass Ti powders were sedimented and finer particles smaller than 1 μm was removed.

4.1.2. Sintering methods

After compacting by CIP, sintering was done in vacuum or inert gas atmosphere (Ar). As method for sintering (1) electric furnace heating, (2) high frequency induction heating, (3) spark plasma sintering (SPS) were used.

(1) The most common method for sintering is electric furnace heating. CIP compacting with 400 MPa was not enough for sintering of Ti. The 700–1000 MPa CIP pressure was preferable. Heating at more than 1300 °C was necessary for sintering of Ti in vacuum. Under this condition HAP became unstable and decomposition began to occur. Heating is done in the mode from the outside of specimens. Expansion and contraction initiates at surface during heating and cooling process. Internal stress tends to be induced more, especially in the cooling process, which is another cause to produce the delayed fracture with higher probability. The product of FGM up to 30HAP could be stably formed, but Ti/100HAP was resulted in autodestruction.

(2) High frequency induction heating can heat to high temperature enough for sintering of Ti and HAP easily. Sintering can be finished quickly. Ti or other metal particles are heated by itself from the inside, therefore the internal stress due to thermal expansion and contraction may be relatively less produced and it is favorable for sintering of Ti whose surface is covered with strong oxide layer. In principle only metals are heated and heat is not generated in ceramics. This may help to make the decomposition of HAP relatively less and could make the stable FGM. However HAP content is limited up to 30 wt.% in our experience and up to 50 wt.% if Ti wire is inserted in the center core of 2–3 mm. cylinder. It was not possible to fabricate FGM from pure Ti to 100%HAP.

(3) SPS can heat both metal and ceramics, even polymers. One may also expect further effects such as spark plasma between particles. This may break the surface oxide layer of Ti, enhance sintering, and lower the sintering temperature and the decomposition of HAP. The stable Ti/HAP FGM endurable to machining and animal implantation test followed by specimen prepara-

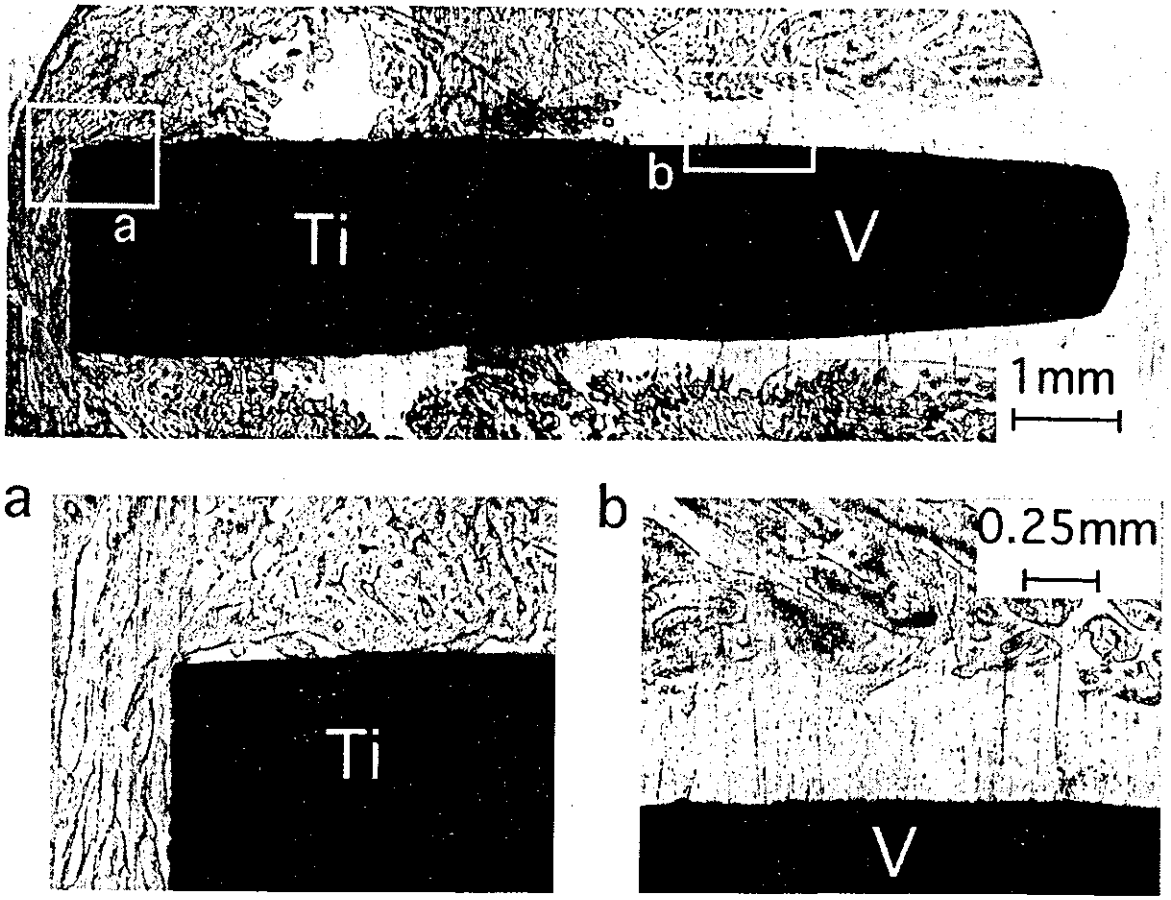

Fig. 11. Histological observation of bone formation and resorption around Ti|V biimplant inserted in tibia of rabit for 4 weeks. New bone was formed directly contact to Ti (a), while juvenile immature bone was formed apart from V (b).

tion including diamond saw cutting and polishing could be realized by sintering at 850 °C much lower than 1300 °C in the conventional sintering method. Raman spectra from 100%HAP area showed the prominent peak of OH. around 3550 cm^{-1}, which does not necessarily appear in many hydroxyapatites and implies the excellent crystallization [18].

However this is still the compromise to sacrifice to some extent the full sintering. To enhance the sintering effect the sintering pressure was increased from 20 to 40 MPa and further to 80 MPa. The attainment of higher SPS pressure is controlled by the strength of mold material rather than the pressing capacity of SPS instrument. At higher than 650 °C the creep deformation occurs in the hard metal WC–Co alloy. By use of high strength graphite 80 MPa was possible to impose instead of 20 MPa using the ordinary graphite [17,18].

4.2. Imaging of FGM structure

Various imaging methods [26–30] were applied to observe and evaluate the functionally graded structure and tissue reaction around implant inserted in animal experiment [13,15]. After the external appearance was observed either with the naked eye or by optical microscopy, X-ray tranmission image [11] was taken. The cross section was investigated by secondary electron image and compositional image [1,11,30] using the reflection electrons in SEM. The FGM specimens intentionally without the deposition of metal coating layer on surface were also used in the observation of the usual seconary electron image in SEM. HAP is electronically nonconductive and exhibits the excess brightness by electron charging effect in SEM observation, which makes easier recognition of HAP particles in the Ti matrix [12]. Line analysis and elemental mapping was done by EPMA and XSAM [11–13,20–22].

The optical image is based on the reflection and scattering of light, dependent on surface morphology. X-ray transmission and reflection electron images are based on the absorbance and reflectivity which are dependent on atomic number. Line analysis and mapping is based on characteristic X-ray emission. All these methods were used to confirm the gradient structure.

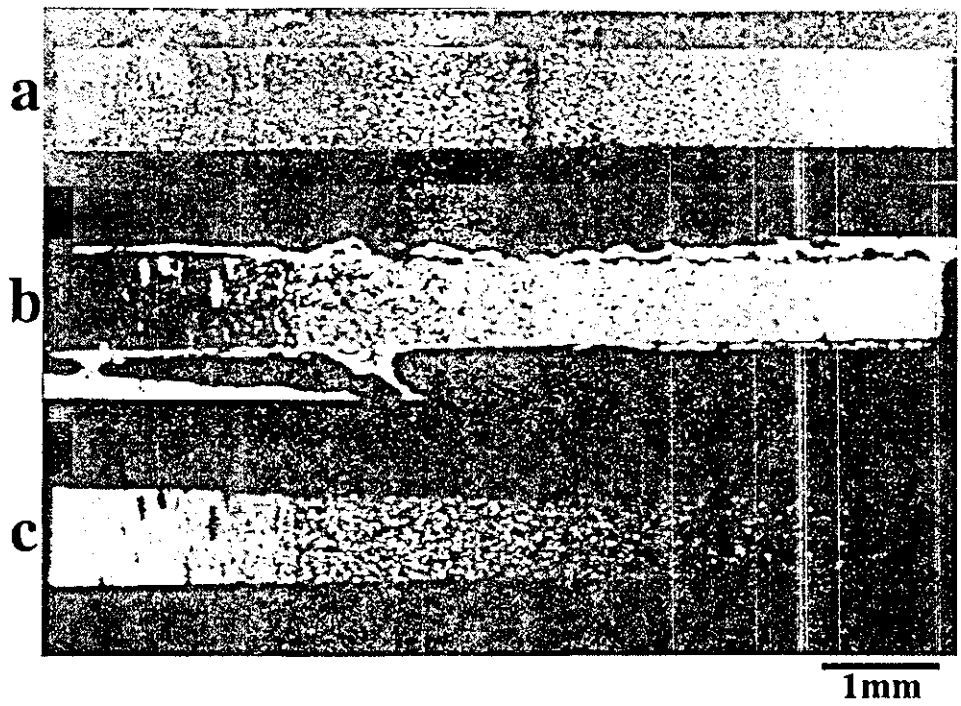

Fig. 12. Ti/HAP FGM implant made by SPS after three point flexural test (a) and Ca (b), Ti (c) mappings by EPMA after 8 week insertion in bone marrow of femora of rat.

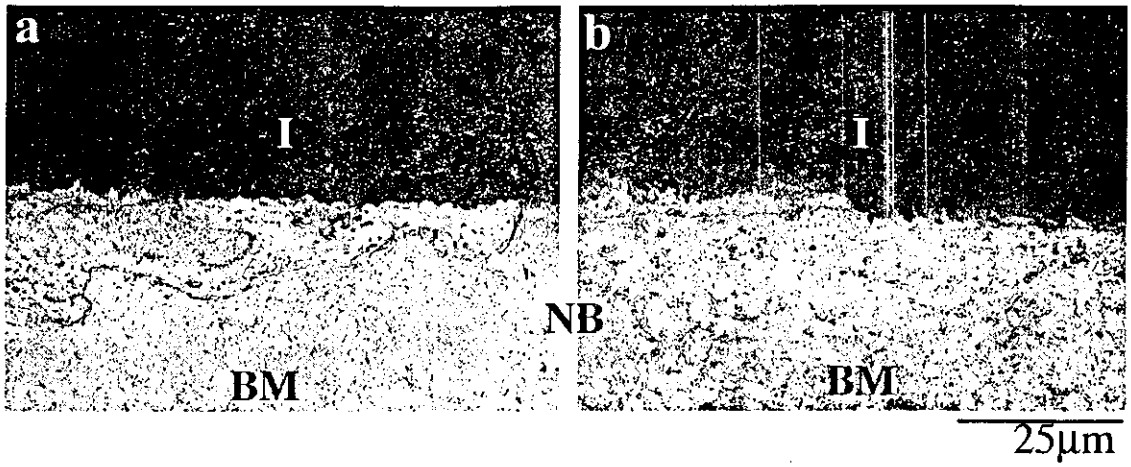

Fig. 13. Histological image around the Ti side (a) and the HAP-rich side (b) in the Ti/HAP FGM implant inserted in femora of rat for 16 weeks. I: implant, NB: new bone, BM: bone marrow.

For the observation of new bone formation around the implant which was inserted in the femora of rats, the compositional image by reflection electrons [1,11,30] and elemental mapping by EPMA and XSAM [11–13,20–22] were applied as well as the conventional method to observe histologically the stained thin specimen by optical microscopy. The contrast of those imaging methods is based on the electronic structure of specimens. Specimen preparation is simple without the ultra thin sectioning and staining. The recognition and evaluation of new bone area is easy. The light microscopic image of the stained tissue obtained by conventional means presents some ambiguity in tissue interpretation, depending on the degree of staining. Therefore, the substantial experience is necessary for proper interpretation of the observed features. On the other hand, the bone region is unambiguously evident in the Ca mapping, providing a basis for clear interpretation. The mapping method also can provide the distribution of each component element.

The difference in the distribution density of component atoms and of the resulting ratio of one element to

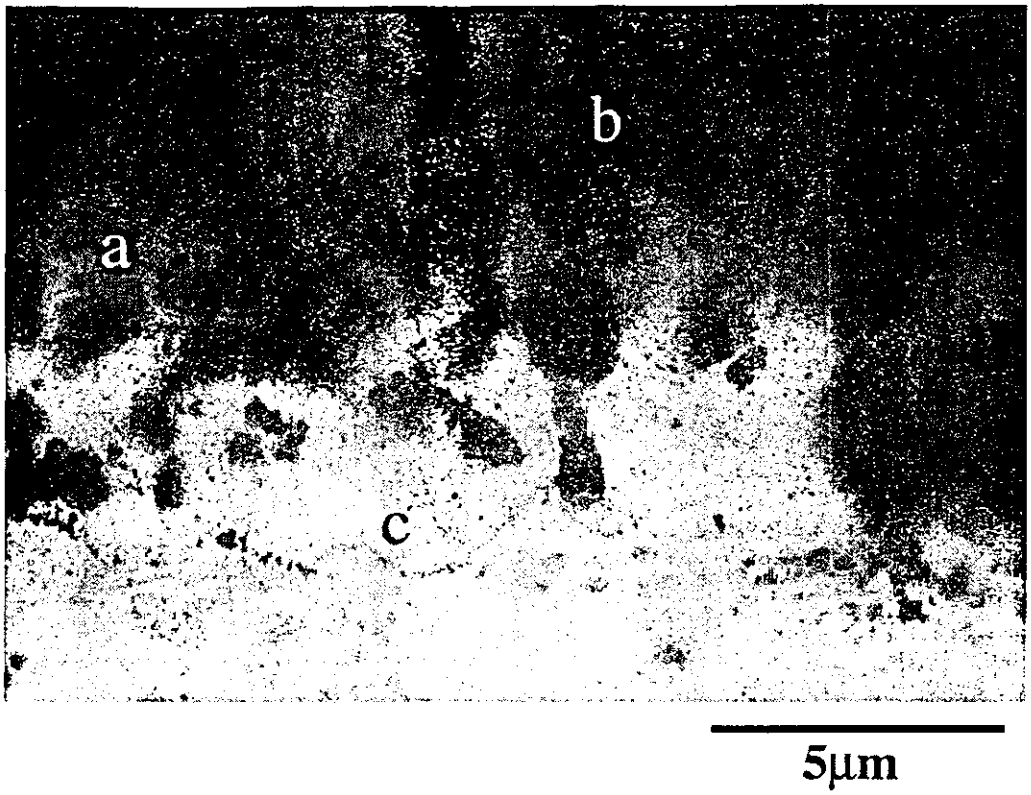

Fig. 14. Enlargement of new bone formation around HAP rich region of Ti/HAP FGM: a: HAP matrix, b: Ti particles, c: new bone.

another also can be obtained. In bone formation and apatite ceramics, the ratio of Ca/P in a wide range of non-stoichiometric compositions is often of major interest. It is possible to obtain such elemental ratio using the elemental analysis and mapping method. The typical example is found in Fig. 3 where dephospored region was visualized. XSAM was more sensitive to the heavier elements such as Ni and Co [21] shown in Figs. 8 and 12, although the spatial resolution was 100 μm or 10 μm, much lower than 1 μm in EPMA. On the other hand, the different tissues can be distinguished by the usual histopathological method which uses staining and light microscopic observation. Therefore the combination of histological observation and elemental mapping techniques could lead to the clear interpretation of the observed microstructural tissue, together with the additional information about the components.

4.3. Mechanical properties

The measurement of the properties of the uniform Ti–HAP specimens made by SPS showed that the density is very close to the true density, and the fracture toughness increases remarkably with the addition of Ti from 0.7 MPa·m$^{1/2}$ of pure HAP to 3.8 MPa·m$^{1/2}$ of Ti–50 vol.% HAP [19]. The addition of Ti to HAP had much effect on the increase of fracture toughness and other mechanical properties. Compression strength of bone is approximately 150 MPa. The Ti/20HAP FGM has approximately the comparable strength.

For Ti/100HAP FGM decomposition effect in sintering process is not negligible. Internal stress also arises from the difference of sintering shrinkage and thermal expansion coefficient at the interface from one region to others. To avoid autodestruction sintering temperature was lowered by use of SPS. There was much improvement in sintering by SPS compared with the conventional CIP and furnace sintering method. SEM observation showed that SPS can enhance the sintering effect in spite of the lower sintering temperature.

It is, however, still the compromised condition and sintering is imperfect. Ti–HAP composite is in a first approximation the physical mixture of both particles and there is no binding force between Ti and HAP particles. The strength of 60–90HAP region is not sufficient. Fracture of FGM occurs near the weakest region or its neighbor. In the three point flexural test of Ti/HAP FGM prepared with the SPS pressure 40 MPa, fracture occurred, deviated from center, in the HAP-rich side which is weaker. In the FGM prepared with 80 MPa, fracture occurred inside the single layer in the center. The flexural strength was increased to 36 MPa and the compressive strength 88 MPa, respectively.

The strength obtained here is not enough for practical use at moment. One of the reasons other than decomposition problem is the widest composition gradient

from 0 to 100% HAP, which is the most difficult to attain the perfect properties. If the range of gradient is limited up to 40% as shown in Fig. 7, it has enough strength durable to the clinical practice.

The decreasing tendency of hardness to the direction of tooth root region in Fig. 5b would contribute to the stress relaxation, which would relieve jaw bone from damage by imposition of high spike of impact stress on implant.

4.4. Biocompatibility

HAP is the main component of hard tissue such as bone and teeth. Ti is one of the best biocompatible metals and is commonly used for implant. Co is an important alloying element in non-precious dental alloys. Co–Cr is used for denture and orthodontic wire. Nickel, one of the major alloying elements for industrial materials such as stainless and Ni–Cr, is a typical element to evoke an allergic reaction. Ni–Cr alloy, which used to be a popular dental material, is now decreased in its usage in dentistry. Ni as an alloying element is mostly substituted by Co. Ni–Ti is used as orthodontic wire for initial treatment of leveling the irregular teeth row, utilizing its superelasticity as one variant phenomenon of shape memory effect. Ag is an important alloying elements of dental alloys. It is also often used as anti-bacterial materials. These materials as well as other refractory metals were used for implantation and compared to see the effect on tissue response.

No inflammation was observed for Ti implant inserted in soft tissue after one week. The histological observation of stained specimen by optical microscopy showed that the thin fibrous connective tissue was formed uniformly, surrounding an implant with constant thickness. Refractory metals of Ti, Zr, Hf, Nb, Ta except V in the IVa and Va groups, Re in the VIIIa group [1], Ti (N) [31,32] and TiN showed very little inflammatory reaction in animal experiments both in hard tissue and in soft tissue. Dissolution of these elements into tissue was not observed by elemental mapping. They have sufficient biocompatibility with a slight difference in new bone formation around implant in hard tissue.

Ni, implanted in soft tissue, induced severe inflammation [20]. The inflammatory area was coincided with the dissolved region of Ni revealed by Ni mapping of XSAM as seen in Fig. 8. There was relation between the gradient concentration of dissolved Ni and the degree of degeneration in soft tissue as a function of distance from Ni implant surface.

Although Fe was dissolved most of all metals tested in the present paper with the difference of more than one order, tissue did not suffer the serious inflammation (Fig. 9). The formation of fibrous connective tissue surrounding implant was observed in the early stage in Fe, while slightly delayed in Ag and stainless steel (SUS316), which reflects the difference of biocompatibility sensitively.

In the case of the implantation test of Ti/Co FGM [16] into soft tissue (Fig. 10), the thin fibrous connective tissue with the thickness of a few layers of fibroblast was formed at the side of pure Ti. The tissue layer thickness increased gradually with the Co concentration, forming more inflammatory tissue in the Co rich region, although tissue was not so severely deteriorated in Co as in Ni. The dissolved region of Co revealed by XSAM mapping and the inflammatory tissue region were in accordance with each other. The change of concentration of Co affected on the biocompatibility, which caused the change of tissue response. In Ti|V biimplant inserted in the tibia of rabit the new bone formation was severely depressed in the V side.

Co caused inflammatory change, while Ni exhibited severe degeneration and necrosis. In both elements the dissolved region and the inflammatory tissue region were corresponded each other. The tissue reacted gradiently in response to the gradient composition of FGM materials. Epple et al. used the Ni/Ti FGM to evaluate the cytotoxicity for different composition with a single specimen [33]. Their in vitro test also showed the gradient cell reaction.

The difference in bioreaction was relatively easy to recognize for the combination of biocompatible and biomalignant materials as in the case of Ti/Co FGM implant in soft tissue and Ti|V biimplant in hard tissue. It was difficult, however, to show the difference for the combination of biocompatible materials. In the implantation test of Ti/20HAP FGM into hard tissue there was only minor difference in new bone formation between the pure Ti region and the HAP-rich region. This is primarily because both Ti and HAP have good biocompatibility. In such a case the influence of other factors are often dominant. The new bone formation is easily affected by the shape, porosity, surface roughness of implants, the inserted position, distance from cortical bone and perforated region, and individual difference of animals other than implant materials.

It was shown that the coexistence of the HAP component seemed to induce the effect to accelerate the formation of new bone from the earlier stage under the ideal experimental conditions for Ti/100HAP. Fig. 14 showed that the maturation of new bone preceded in the HAP-rich region. This effect worked gradiently to the graded composition of Ti/HAP FGM implant.

The both gradient reactions to FGM, formation of fibrous connective tissue in soft tissue and osteogenesis in hard tissue, imply thus the possibility to control the tissue response over mm to μm scales in each part through the designed gradient composition and structure of FGM implant. This would contribute to the application of biomaterials for use as artificial internal organs.

Brinell hardness of Ti/HAP FGM decreased from 61 in pure Ti to 15 in pure HAP as shown in Fig. 5b. Although the hardness in HAP region is not sufficient for practical use, the decreasing tendency of hardness toward the tooth root contributes to stress relaxation in the implanted region of bone.

The gradient functions in both the biochemical affinity to osteogenesis and the mechanical properties with stress relaxation effect could contribute to the efficient biocompatibility. We may also include other functions for functionally graded implant such as abrasion resistance which is important in the artificial joint and abutment part in dental implant [31,32] to avoid the cytotoxicity by minute particles, originated from their size effect [34,35].

5. Conclusions

1. Ti/HAP and other FGM specimens were fabricated by powder metallurgy to optimize both mechanical properties and biocompatibilities.
2. Electric furnace heating, high frequency induction heating and spark plasma sintering (SPS) methods were used for sintering and compared. The stable Ti/HAP FGM implant could be successfully fabricated by application of SPS.
3. Ti/HAP showed that the maturation of newly formed bone was preceded in the HAP rich region.
4. The gradient functions in both the biochemical affinity to osteogenesis and the mechanical properties with stress relaxation in Ti/HAP FGM could attain the efficient biocompatibility for implant.
5. The study demonstrated that the tissue reaction changes gradiently in response to the gradient composition or structure of materials. This implies the possibility to control the tissue response by functionally graded structure of biomaterials.

Acknowledgements

Research was performed under Grant-in-Aid for Scientific Research (B)(2) from the Ministry of Education, Science, Sports and Culture of Japan, and Health and Laybour Sciences Research Grants in Research on Advanced Medical Technology from the Ministry of Health, Laybour and Welfare of Japan. The authors are grateful to Dr. Koichi Omamyuda of Sumitomo Osaka Cement for the supply of HAP.

References

[1] Matsuno H, Yokoyama A, Watari F, Uo M, Kawasaki T. Biocompatibility and osteogenesis of refractory metal implants, titanium, hafnium, niobium, tantalum and rhenium. Biomaterials 2001;22:1253–62.
[2] Driessens FCM, Verbeeck RMH. Biominerals. Boca Raton: CRC Press; 1990.
[3] Aoki H. Science and medical application of hydroxyapatite. Tokyo: Japanese Association of Apatite Science; 1991.
[4] Aoki H. Medical applications of hydroxyapatite. Tokyo: Ishiyaku EuroAmerica; 1994.
[5] Uo M, Mizuno M, Kuboki Y, Makishima A, Watari F. Properties and cytotoxicity of water soluble Na..O-CaO-P..O.. glasses. Biomaterials 1998;19:2277–84.
[6] Imai T, Watari F, Yamagata S, Kobayashi M, Nagayama K, Nakamura S. Mechanical properties and estheticity of FRP orthodontic wire fabricated by hot drawing. Biomaterial 1998; 19(23):2195–200.
[7] Watari F, Yamagata S, Imai T, Nakamura S, Kobayashi M. The fabrication and properties of aesthetic FRP wires for use in orthodontics. J Materials Science 1998;33:5661–4.
[8] Hirai T. Functionally gradient materials. In: Cahn RW, Haasen P, Kramer EJ, editors. Materials science and technology, vol. 17B: processing of ceramics part 2. Weinheim: Verlagsgesellschaft; 1996. p. 293–341.
[9] Takahashi H, Watari F, Nishimura F, Nakamura H. Functionally gradient materials of titanium-apatite and titanium-silica for dental use. J Jap Soc Dental Mater Devices 1992;11(3):462–8 [in Japanese].
[10] Watari F, Yokoyama A, Saso F, Uo M, Kawasaki T. Functionally gradient dental implant composed of titanium and hydroxyapatite. In: Ilschner B, Cherradi N, editors. Proc. 3rd Int. Symp. Structural & Functional Gradient Materials. Lausanne: Polytech. Univ. Romand; 1995. p. 703–8.
[11] Watari F, Yokoyama A, Saso F, Uo M, Kawasaki T. Elemental mapping of functionally graded dental implant in biocompatibility test. In: Shiota I, Miyamoto Y, editors. Functionally graded materials 1996. Amsterdam: Elsevier; 1997. p. 749–54.
[12] Watari F, Yokoyama A, Saso F, Uo M, Kawasaki T. Fabrication and properties of functionally graded dental implant. Composites Part B 1997;28B:5–11.
[13] Watari F, Yokoyama A, Saso F, Uo M, Matsuno H, Kawasaki T. Imaging of gradient structure of titanium/apatite functionally graded dental implant. J Jpn Inst Metals 1998;62(11):1095–101 (in Japanese).
[14] Watari F, Yokoyama A, Saso F, Uo M, Matsuno H, Kawasaki T. Biocompatibility of titanium/hydroxyapatite and titanium/cobalt functionally graded implants. In: Kayser WA, editor. Functionally Graded Materials 1998. Zurich: Trans Tech Publications; 1999. p. 356–61.
[15] Watari F, Yokoyama A, Saso F, Matsuno H, Uo M, Kawasaki T. Biocompatibility and bioreactivity of Ti-based functionally graded implant. In: Vincenzini P, editor. Advances in science and technology (Proc. 9th CIMTEC-World Forum on New Materials), vol. 28. Materials in clinical applications. Faenza: Techna Srl; 1999. p. 245–50.
[16] Watari F, Yokoyama A, Matsuno H, Miyao R, Uo M, Tamura Y, Kawasaki T, Omori M, Hirai T. Gradient tissue reaction induced by functionally graded implant. In: Trumble K, Bowman K, Reimanis I, Sampath S, editors. Functionally graded materials 2000, ceramic transaction 114. Am. Ceramic Soc; 2001. p. 73–80.
[17] Watari F, Yokoyama A, Matsuno H, Miyao R, Uo M, Kawasaki T, Omori M, Hirai T. Fabrication of functionally graded implant and its biocompatibility. In: Ichikawa K, editor. Functionally graded materials in the 21st century: a workshop on trends and forecasts. Boston: Kluwer Academic; 2001. p. 187–90.

[18] Watari F, Kondo H, Miyao R, Omori M, Okubo A, Hirai T, Yokoyama A, Uo M, Tamura Y, Kawasaki T. Effect of spark plasma sintering pressure on the properties of functionally graded implant and its biocompatibility. J Jpn Soc Powder Powder Metallurgy 2002;49(12):1063–9 [in Japanese].

[19] Yokoyama A, Watari F, Miyao R, Matsuno H, Uo M, Kawasaki T, Kohgo T, Omori M, Hirai T. Mechanical properties and biocompatibility of titanium-hydroxyapatite implant material prepared by spark plasma sintering method. In: Proc. 13th Int. Symp. Ceramics in Medicine, Bologna, Italy, 22–26 Nov. 2000. Key Engineering Materials vols. 192–195, 2001. p. 445–8.

[20] Uo M, Watari F, Yokoyama A, Matsuno H, Kawasaki T. Dissolution of nickel and tissue response observed by X-ray analytical microscopy. Biomaterials 1999;20(8):747–55.

[21] Uo M, Watari F, Yokoyama A, Matsuno H, Kawasaki T. Visualization and detectability of rarely contained elements in soft tissue by X-ray scanning analytical microscopy and electron probe micro analysis. Biomaterials 2001;22:1787–94.

[22] Uo M, Watari F, Yokoyama A, Matsuno H, Kawasaki T. Tissue reaction around metal implants observed by X-ray scanning analytical microscopy. Biomaterials 2001;21:677–85.

[23] Matsuo S, Watari F, Ohata N. Fabrication of functionally graded dental composite resin post and core by laser lithography and finite element analysis of its stress relaxation effect on tooth root. Dental Mater J 2001;20(4):257–74.

[24] Satoh N, Ueda Y, Yorimoto T, Aida H, Matsuo S, Ohata N, Watari F. Firing shrinkage of porcelain-resin composites prepared by laser lithography. Dental Mater J 1999;18(4):444–52.

[25] Konishi J, Watari F, Kawamoto C, Sano H. Effect of sphericalyzed particles on the firing contraction of porcelain inlay processed by cold isostatic pressing. J Biomed Mater Res 2003;66B:553–8.

[26] Watari F, Cowley JM. The study of oxide formation on (001), (011), (111) and (113) surfaces of Cr thin films using STEM-microdiffraction methods. Surface Science 1981;105:240–64.

[27] Watari F, Delavignette P, Van Lunduyt J, Amelinckx S. Electron microscopic study of dehydration transformations III: high resolution observation of reaction process: FeOOH..Fe2O3. J Solid State Chemistry 1983;48:49–64.

[28] Kobayashi Y, Ohshima Y, Ikeda T, Komatsu H, Watari F, Shimokobe H. AFM and SEM observation of morphological changes of human dentin surface by treatment of acidic agents. Dentistry in Japan 1995;32:46–51.

[29] Watari F. In situ etching observation of human teeth in acid agent by atomic force microscopy. J Electron Microscopy 1999; 48(5):537–44.

[30] Watari F. Compositional and morphological imaging of laser irradiated human teeth by low vacuum SEM, confocal laser scanning microscopy and atomic force microscopy. J Mater Sci Med 2001;12:189–94.

[31] Tamura Y, Yokoyama A, Watari F, Uo M, Kawasaki T. Mechanical properties of surface-nitrided titanium for abrasion resistant implant materials. Materials Transactions 2002;43(12): 3043–51.

[32] Tamura Y, Yokoyama A, Watari F, Kawasaki T. Surface properties and biocompatibility of nitrided titanium for abrasion resistant implant materials. Dental Mater J 2002;21(4):355–72.

[33] Bogdansky D, Kller M, Mller D, Muhr G, Bram M, Buchkremer HP, Stver D, Choi Jongsik, Epple M. Easy assessment of the biocompatibility of Ni-Ti alloys by in vitro cell culture experiments on a functionally graded Ni-NiTi-Ti material. Biomaterials 2002;23:4549–55.

[34] Kumazawa R, Watari F, Takashi N, Tanimura Y, Uo M, Totsuka Y. Effects of Ti ions and particles on cellular function and morphology of neutrophils. Biomaterials 2002;23:3757–64.

[35] Tamura K, Takashi N, Kumazawa R, Watari F, Totsuka Y. Effects of particle size on cell function and morphology in titanium and nickel. Materials Transactions 2002;43(12): 3052–7.

Key Engineering Materials Vols. 254-256(2004) pp. 919-922
online at http://www.scientific.net

Effects of Micro/Nano Particle Size on Cell Function and Morphology

K. Tamura[1], N. Takashi[1], T. Akasaka[2], I. D. Roska[2], M. Uo[2],
Y. Totsuka[1], F. Watari[2]

[1] Department of Oral and Maxillofacial Surgery, Graduate School of Dental Medicine,
tam@den.hokudai.ac.jp
[2] Dental Materials and Engineering, Graduate School of Dental Medicine,
Hokkaido University, kita 13 nishi 8, kita-ku, Sapporo, 060-8586, Japan

Keywords: particle, biomaterial, titanium, titanium dioxide, carbon nanotube, biocompatibility

Abstract. The cytotoxicity of micro/nano particles in Ti, TiO and carbon nanotube was investigated by in vitro biochemical analyses using human neutrophils. The particles smaller and larger than the neutrophils were used to determine the relationship between cell and particle size with respect to cytotoxicity. As the particle size decreased, the cell survival rate was decreased and, with the good corresponding relation to this, the value of lactate dehydrogenase (LDH), which is the indication of cell disruption, was increased. The release of superoxide anion showed the increasing tendency. Proinflammatory cytokines were detected distinctly for 3μm or smaller particles and very little in more than 10μm, which is closely related to the phagocytosis by neutrophils. ICP elemental analysis showed that the dissolution from Ti particles was below detection limit. Micro and nano particles stimulated the cell reactions according to the results of the human neutrophil functional tests. As the particle size was smaller, the inflammation was pronounced. The fine particles less than 3μm caused distinctly the inflammation in the surrounding tissue. All these results indicated that the cytotoxicity was induced due to the physical size effect of particles, which is different from the ionic dissolution effect. The clinical phenomenon confirmed the result obtained in vitro cell tests. The neutrophils stimulated by fine particles may cause the inflammatory cascade and harm the surrounding tissue.

Introduction

Ti and its alloys are the commonly used material in plastic surgery because it is one of the most biocompatible metals [1,2]. Ti is highly corrosion-resistant at ambient temperature due to its thin and stable protective oxide layer formed on its surface. In this sense Ti is the ideal metallic material for implant [3,4]. However, it is clinically reported that the abraded fine titanium particles produced in sliding parts of artificial joints often caused inflammation in the surrounding tissue [1,2]. However, little is known about the effect of micro/nano particles on cellular function and the relevance between *in vivo* and *in vitro* findings. The purpose of this study is to analyze the vital reactions of human neutrophils to the Ti, TiO_2 particles and carbon nanotubes and their size effect.

Materials and probe cells

The dependence of cytotoxicity on particles size in titanium, titanium oxide (TiO_2) and carbon nanotubes was investigated by biochemical functional analysis and by microscopic observation of cellular morphology.

Particles. The Ti, TiO_2 and carbon nanotubes particles colloid solutions were prepared. ICP elemental analysis showed that the dissolution from Ti particles were below detection limit. The carbon nano-tubes is 99% purity. The solubilization distributed processing was carried. The average diameter and size distribution of the TiO_2 particles and carbon nanotubes were determined by electron microscopy (SEM) and by laser scattering particle distribution analyzer (SALD-7000, Shimadzu).

The various sizes of Ti, TiO_2 and carbon nanotubes particles were mixed with HBSS (Hanks' balanced salt solution). The colloid solutions were adjusted to PH 6.8 by 1N NaOH solution, sterilized by autoclave and dispersed by sonicator [5,7].

Cells. Human peripheral blood was obtained from healthy volunteers in our group. Neutrophils were separated from the blood using the 6% isotonic sodium chloride containing the hydroxyethyl starch and lymphocyte isolation solution (Ficoll-Hypaque)[6,7]. The cells were maintained in HBSS. After particles were kept dispersed, neutrophils were added, and incubated in a humidified atmosphere of 5% carbon dioxide at 37 °C for 60 minutes. The experiments were performed using cells within 3 hours after collection of blood and the cell density was adjusted to 10^6 cells / ml [7].

Methods

Cell survival rate, leakage of lactate dehydrogenase (LDH), product of superoxide anion, and release of cytokines of tumor necrosis factor-alpha (TNF-alpha), interleukine-1 beta (IL-1beta) were measured to analyze biochemical reaction.

(1) Cell survival rate: The cell stained with trypan blue population was counted under an optical microscope using Thomas' hemacytometer. The number of vital cell in the control specimen was considered as 100%.

(2) LDH activity: The LDH values of samples were measured using the lactate dehydrogenase C test kit (Wako Pure Chemical Industries) and by spectrophotometry.

(3) Superoxide anion production: Superoxide anion (O_2^-) was assayed by measuring the superoxide dismutase-inhibiting reduction of equine ferricytochrome C (550 nm). The reaction was promoted by adding 1.39mM PMA (phorbol 12-myristate 13-acetate) [7].

(4) Cytokine release: TNF-alpha and IL-1 beta in the supernatant was measured using ELISA kits (Endogen) [7].

The values are expressed as means +/- standard deviation (n=6). Data were analyzed by Student's-t test with the level of significance set at 5%.

The pathological and morphological changes were observed by optical microscopy and SEM.

Results

Ti particles diameter were 3, 10, 50, and 150 μm and TiO_2 particles were 0.05, 0.5, and 3 μm in average size, as confirmed by SEM and the particle distribution analyzer. The SEM image shows carbon nanotubes with diameter of 20 nm and length of 100 nm.

The significant difference of the survival rate from control was observed in all nano particles (Fig.1). The Ti micro particles showed clearly the size dependency. The cell survival rate decreased, when the particle size became smaller. The nanoparticle of TiO_2 also showed the similar tendency. The lowest mean value of the survival rate was 84.6% in the size 50 nm for TiO_2 particles, which were the smallest particles in this study.

LDH showed the tendency to increase as the particle size became smaller (Fig.2). The LDH level of 147.2 Wroblewski unit was significantly higher in the 50 nm than the other larger sizes.

The neutrophils stimulated by the 3 μm or less particles showed the large productions of superoxide anion. The other larger size particles were slightly higher than control solutions (Fig.3).

There is a clear difference in the emission of inflammatory cytokines for 3 μm and 10 μm (Fig.4). The distinct release of TNF- alpha was observed in 3 μm or less particles. There was no statistical difference of cytokines under 3 μm. The IL-1beta showed the similar

SEM observation revealed the degenerative changes in the morphology of neutrophils (Fig.5). The activated neutrophils extended some pseudopods and phagocytized particles into the cytoplasm. 50nm TiO_2 particles and carbon nanotube induced the morphological change of neutrophils. After 6 hours, the atrophied and destroyed neutrophils were observed.

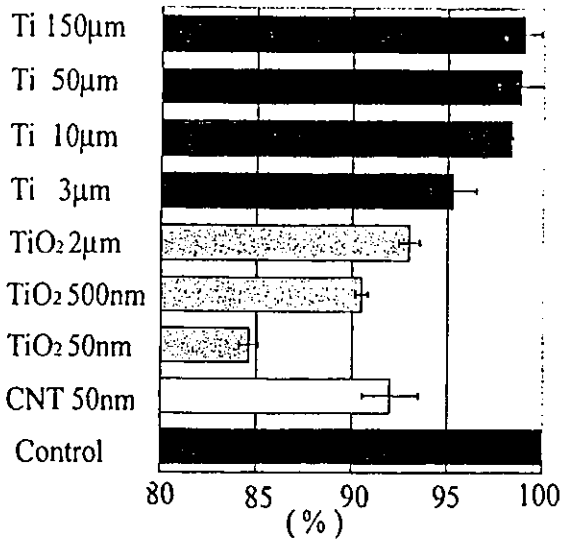

Fig.1 Cell survival rate

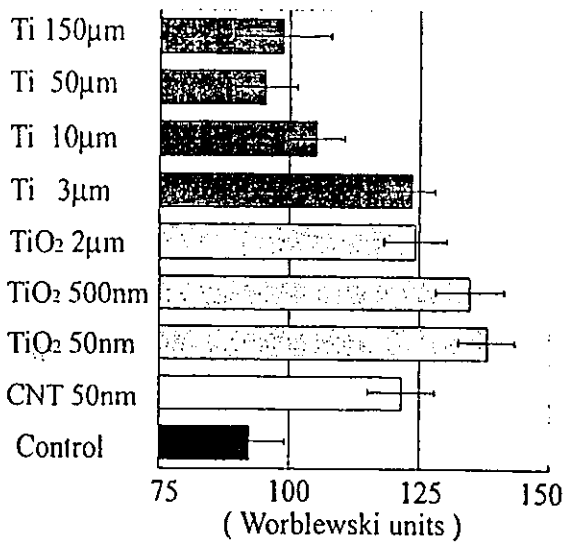

Fig.2 LDH activity

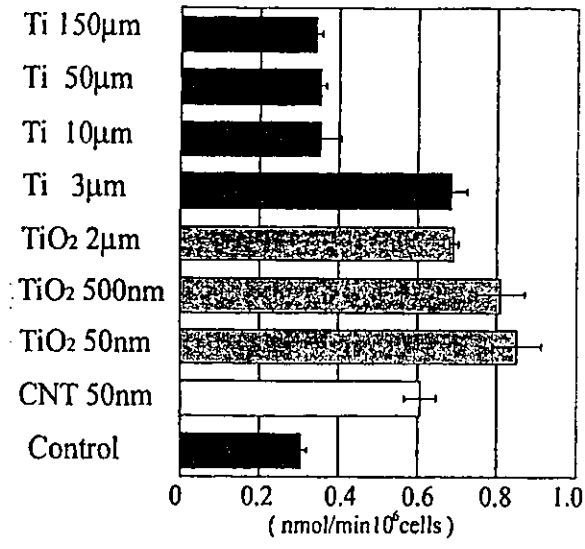

Fig.3 Superoxide anion

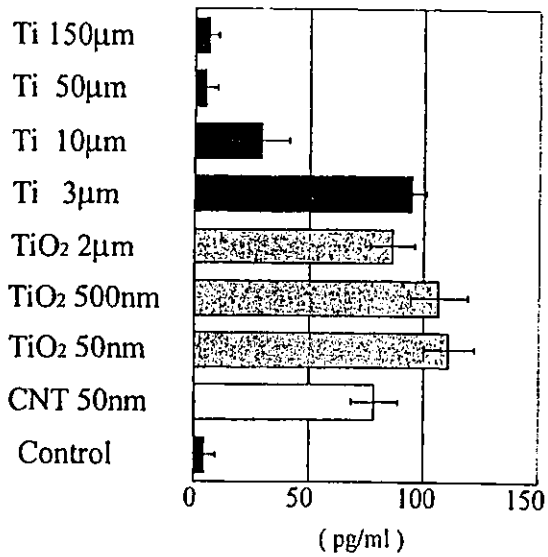

Fig.4 TNF-alpha

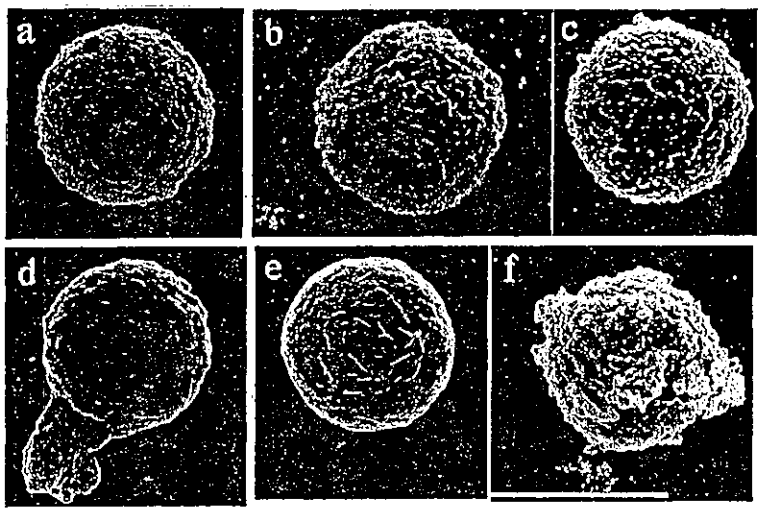

Fig.5
SEM images of morphological change of neutrophils
(Bar = 10 μm)
a: Neutrophil with HBSS
b: Activated by TiO_2 particles
c: Activated by Carbon nanotubes
d: Extension of pseudopod and phagocytized particles
e: Atrophied neutrophil
f: Destroyed membrane

Discussions

The study clearly showed the cytotoxicity due to the particle size effect in Ti, TiO_2 and CNT. Micro-nano particles may cause cytotoxicity, although the macroscopic size is quite biocompatible. The increased superoxide content in vivo may affect the cell circumference. The chemical mediators, TNF- alpha and IL-1beta, may induce the inflammatory cascade to affect tissue and organ. The effect is further pronounced by phagocytosis when particles are smaller than cells [7]. The clinical inflammation reaction around the abrasion powders can be well understand by the results obtained in cell functional *in vitro* tests.

Acknowledgements

The authors thank Dr. Takafumi Domon, Dr. Ami Fukui, Dr. Kiyomi Tsuji and Dr. Yoshinobu Nodasaka for the valuable advices and preparation of SEM observation, and Dr. Wenzhi Hugetu and Pr. Kazuyuki Touji for supplying the carbon nanotubes.

References

[1] K. Takamura, T. Yamada and Y. Sugioka, et al. : J Biomed Mater Res. Vol 28 (1994), p. 583-9.

[2] Young-kyun Yeo, Seoug-cheul Lim, et al. : J Oral Maxillofac. Surg. Vol 55 (1997), p. 322-326.

[3] A. Rosenberg, K.W. Grätz and H.F. Sailer: J. oral Maxillofac. Surg. Vol 22 (1993), p. 185-188.

[4] Y. Tanimura, F. Watari, et al. : J of Oral and Maxillofacial Surgery. Vol 46(11) (2000), p. 750.

[5] M. Uo, F. Watari, A. Yokoyama, T. Kawasaki, et al. : Biomaterials. Vol 20 (1999), p. 47-55.

[6] F. Takesita, H. Tkata, Y. Ayukawa and T. Suetsugu. : Biomaterials. Vol 18 (1997), p. 21-5.

[7] Kazuchika Tamura, Fumio Watari, et al. : Materials Transactions Vol. 43(12)(2002), p.3052-3057

Materials Transactions, Vol. 45, No. 4 (2004) pp. 1010 to 1014
Special Issue on Frontiers of Smart Biomaterials

Fluorescent Properties of Porcelain-Restored Teeth and Their Discrimination

Kazutoshi Tani[1]*, Fumio Watari[2], Motohiro Uo[2] and Manabu Morita[1]

[1]*Division of Preventive Dentistry, Department of Oral Health Science, Graduate School of Dental Medicine, Hokkaido University, Sapporo 060-8586, Japan*
[2]*Division of Dental Materials and Engineering, Department of Oral Health Science, Graduate School of Dental Medicine, Hokkaido University, Sapporo 060-8586, Japan*

The differentiation of porcelain from tooh using fluorescence emission was investigated as a basic research for the visual detection of porcelain-restored teeth in mass dental health examinations. The fluorescence spectra were taken from the extracted human maxillary central incisors and five types of porcelain by excitation using the light 380-470 nm. There was a clear difference in fluorescence intensity between tooth and porcelain using excitation longer than 400 nm. Tooth and porcelain could be successfully distinguished on an image photographed by fluorescent light.

(Received December 5, 2003; Accepted February 27, 2004)

Keywords: *porcelain, tooth, fluorescence*

1. Introduction

Various aesthetic restorative materials such as composite resin[1-5] and porcelain[6-10] are widely used in dental clinics. Detection of the teeth restored with aesthetic materials has become very difficult for dentists in a mass dental health examination due to the improvement of their aesthetics. The visual inspection of color difference between restorative materials and tooth or exploring of tactile difference of surface quality have been used widely as detection methods of teeth restored with aesthetic materials. However, these detection methods do not have a high degree of reliability, depending on the restored spots of aesthetic materials and examiner's skills and experience. If a clear method for the differentiation of aesthetic materials from tooth with a high reproducibility could be attained, it would be possible to determine easily and precisely the state of the oral health condition of individuals. Our previous study showed that the discrimination of composite resin from the tooth in a resin-restored tooth was possible using the fluorescent properties.[11] In this study, the differentiation of porcelain from tooth was investigated using the fluorescent properties.

2. Materials and Methods

2.1 Measurement of fluorescence spectra

2.1.1 Porcelain samples

Five types of dentin and enamel porcelains were used for the present research (Table 1). All porcelain powders were formed using a steel mold with the dimensions of 10 mm in diameter and a height of 5 mm. Powder compacts were fired according to each manufacturer's recommended firing schedule in a vacuum in a porcelain furnace (CERAMIMAT FA-IV, GC). For enamel porcelain, firing was performed at atmospheric pressure.

2.1.2 Teeth

Four tooth specimens from the human maxillary central incisors without caries or coloring, and tetracycline fluorescence, which had been extracted and stored in 10%-neutral buffer formalin, were prepared.

*Graduate Student, Hokkaido University

Table 1 Porcelains used for measurement of fluorescence.

	Brand name	Manufacture	Shade	Abbreviation
Porcelain	Super porcelain AAA	Noritake	E_1, E_2, E_3, A_1B, A_3B, A_4B, B_1B, B_4B, C_1B, C_4B, D_4B	NTA
	VITA	GC	EN1, A_3	VITA
	ZEOCELIGHT	YAMAMOTO	E3, DA3	ZOC
	VINTAGE UNIBOND	SHOFU	59, A_3B	VT-U
	VINTAGE Halo	SHOFU	59, A_3B	VT-H

The measurement of fluorescence spectra was done with a fluorescence spectrophotometer (F-2500,HITACHI) using the 6 mm × 6 mm frame mask for both the polished surface of porcelain and the flat plane of the labial side of the natural teeth. The fluorescence spectra were measured for the excitation wavelengths of 380, 400, 430, 450 and 470 nm (scan speed 300 nm/min, photo multiplier voltage 700 V, slit width 2.5 nm).

2.2 The fluorescence image

2.2.1 Porcelain restored tooth specimen

After four sound premolar teeth were cut at the root area parallel to the occlusal surface, a cavity of about 3 mm depth was formed using a diamond point (SHOFU 301, 311). An impression of the cavity-formed teeth was taken with silicone rubber impression materials. Four refractory models were made with refractory die materials (Nori-Vest, Noritake). Four porcelain inlays were made by applying a refractory cast according to the manufacturer's recommended methods. Each inlay was fixed in the cavities of the teeth using resin-cement (Super bond, SUN MEDICAL).

2.2.2 Excitation light

Excitation light applied to the porcelain-restored tooth was formed with the combination of a halogen lamp as a light source and various filters. The spectral distribution curve is shown in Fig. 1, which was obtained by multiplying the spectral distribution curve of a light source and the transmission curve of each filter. Filters were fixed on the visible

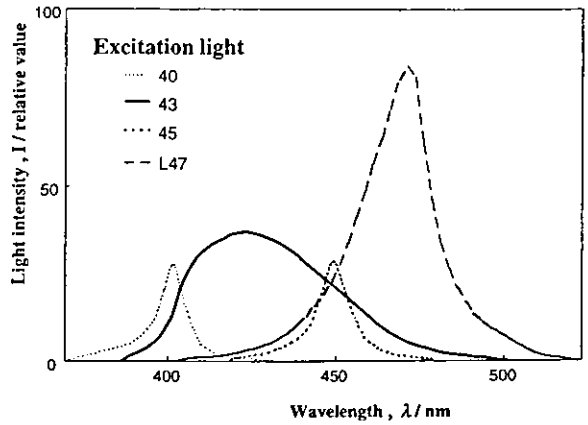

Fig. 1 Spectral distribution curves of excitation lights.

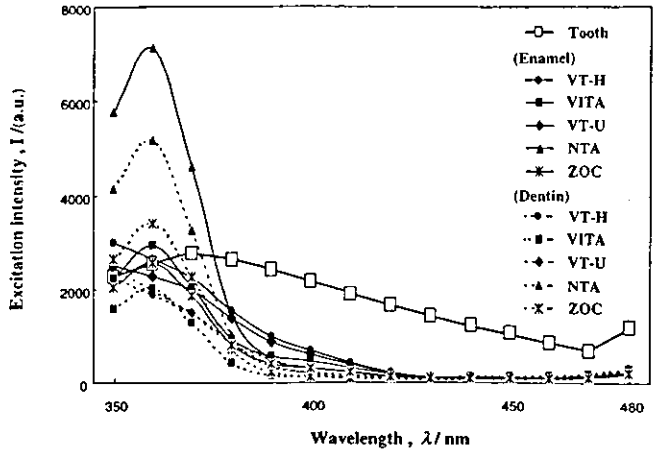

Fig. 2 Excitation spectra of tooth and porcelains at 500 nm fluorescence wavelength.

light-curing unit (JETLITE 3000, J. MORITA) with the wavelength set in the 380~520 nm range, peaking at 480 nm. The excitation light with the peak wavelengths of 400, 430, 450 nm, abbreviated as 40, 43, 45, was formed using the filters HOYA color-glass filter BP-40, FUJIFILM OPTICAL BP-43, HOYA color-glass filter BP-45, respectively. The excitation light L47 used the visible light-curing unit with a blue LED (Radius, OSADA) peaked at 470 nm.

2.2.3 Fluorescent image

Four kinds of porcelain-restored teeth (NTA, VITA, VT-U, VT-H) were set in a dark environment, and were irradiated with the excitation light 40, 43, 45, 47 at a distance of 100 mm and an incident angle of 80°. The filter (HOYA color filter SC-50) with permeability over 500nm was fixed on the camera (Canon EOS100QD). The reversal color film (FUJIFILM PROVIA400) was used to evaluate the efficiency for the discrimination of the porcelain part from the tooth. A monochrome film (NEOPAN SS FUJIFILM) was used to measure the luminance ratio of porcelain and tooth with the filter (HOYA color filter SC-50). A negative film was read as a digital image into a personal computer using the flat scanner, and luminance was measured using image analysis software (Scion-Image). The contrast was calculated as the luminance ratio of porcelain to tooth.

3. Results

3.1 Excitation spectra

The excitation spectra for the 500 nm fluorescence wavelength were shown for dentin and enamel porcelains with the shade A3, the most frequently used color tone in clinics, and tooth in Fig. 2. Tooth showed a broader peak than all other porcelains, peaking around 370 nm. The fluorescence of tooth was stronger than porcelain for the excitation with the wavelengths longer than 380 nm. For excitation less than 380 nm in wavelength, the intensity emitted from tooth was in a similar range as most porcelains.

3.2 Fluorescence spectra

3.2.1 Tooth

The fluorescence spectra of six maxillary incisors at 400 nm excitation were similar, especially for wavelengths longer than 500 nm. This indicated that the conditions for differentiation were constant and reliable in this range.

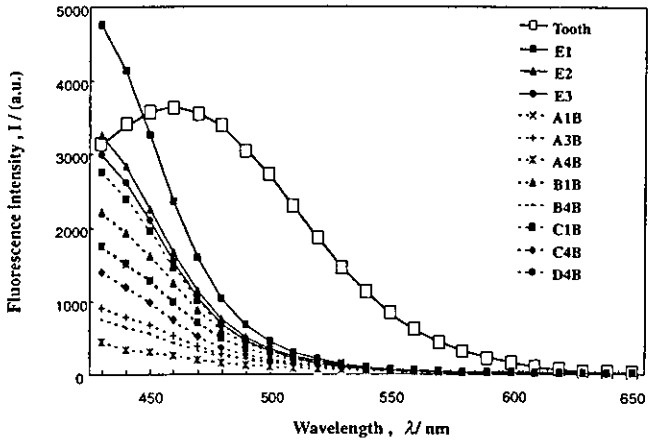

Fig. 3 Difference of fluorescence spectra by color tone of porcelain (Noritake triple A) and spectrum of tooth with 400 nm excitation.

3.2.2 Dependence of fluorescence spectra on shade of porcelain

In Fig. 3, fluorescence spectra at 400 nm excitation for tooth and different shades of super porcelain triple A (NTA, Noritake) were shown: all the three kinds of shades for enamel porcelain (E1, E2, E3) and eight shades selected from sixteen colors for dentin porcelain (A1B, A3B, A4B, B1B, B4B, C1B, C4B, D4B). The fluorescence of tooth was shown as the average intensity of six teeth. The difference in fluorescence was seen depending on each shade in wavelengths lower than 380 nm, and became very small for wavelengths longer than 500 nm.

3.2.3 Comparison of fluorescence of porcelain and tooth

Based on the results of Fig. 3, A3 shade porcelain, most frequently used in clinics, was used as representative in the following. The spectra of tooth and each A3 porcelain at excitation wavelengths of 380, 400, 470 nm are shown in Figs. 4-6. For the 380 nm excitation (Fig. 4), the strongest fluorescence intensity of enamel porcelain showed a similar intensity to tooth, and dentin porcelain was smaller than tooth. The absolute fluorescence intensity of tooth and porcelain at 400 nm excitation decreased compared with

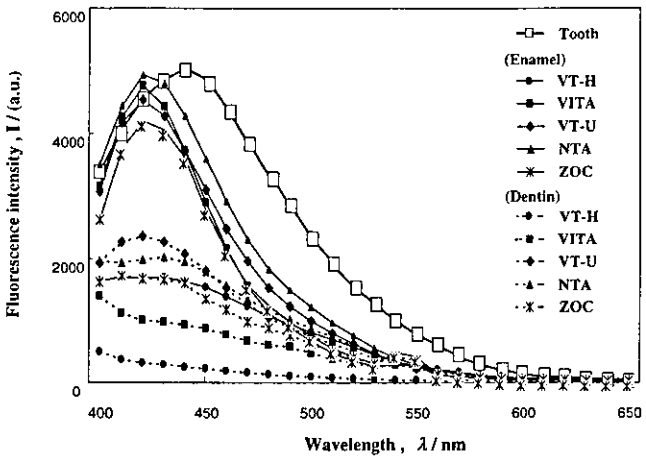

Fig. 4 Fluorescence spectra of tooth and porcelains with 380 nm excitation.

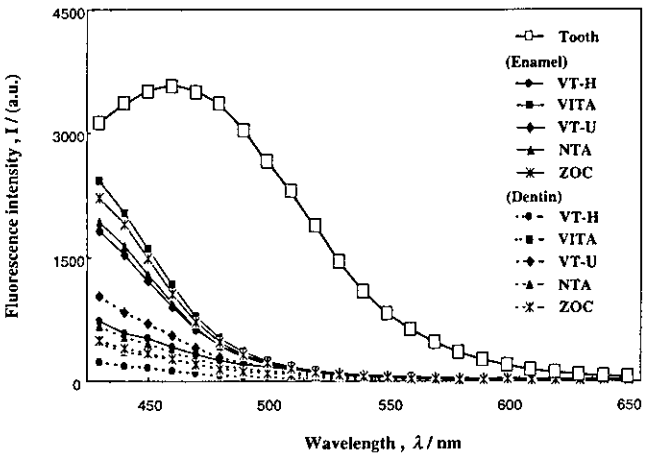

Fig. 5 Fluorescence spectra of tooth and porcelains with 400 nm excitation.

380 nm excitation (Fig. 5). However the relative fluorescence intensity of porcelain was much lower than tooth. As the excitation wavelength becomes longer, reaching 470 nm (Fig. 6), porcelain had very little fluorescence in comparison with 400 nm excitation, although the absolute fluorescence of tooth declined considerably. Fluorescence of porcelain and tooth at 430, 450 nm excitation had the intensity between Fig. 5 and Fig. 6.

3.3 Fluorescent image

Based on the fluorescence spectra, the fluorescent images of porcelain-restored tooth for wavelengths over 500 nm were photographed under the excitation light 40, 43, 45, L47 (Fig. 7). Porcelain ① of Fig. 7 is NTA, ② is VT-U, ③ is VITA, ④ is VT-H. The fluorescence emission of porcelain was weaker than tooth, so that discrimination was possible.

3.4 Contrast evaluation

Monochromatic images for the fluorescence over 500 nm and the luminance ratio of porcelain to tooth are shown for the excitation light 40, 43, 45, L47 in Fig. 8. Under excitation light L47 using the blue the LED, fluorescence intensity of

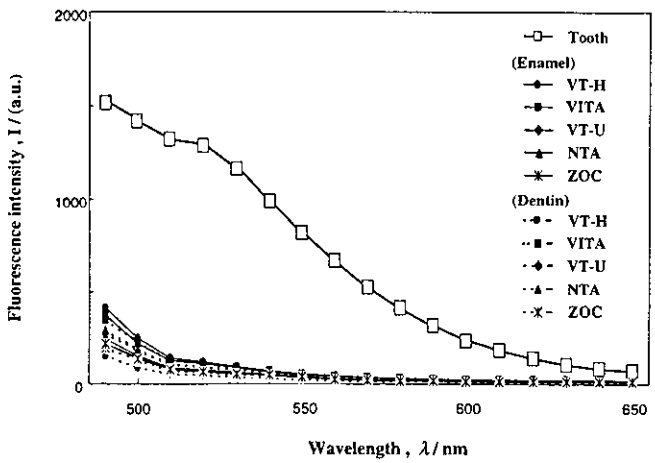

Fig. 6 Fluorescence spectra of tooth and porcelains with 470 nm excitation.

tooth was the strongest. As for the luminance contrast of porcelain to tooth, the excitation light 40 was better than 43, 45, L47.

4. Discussion

4.1 Detection of porcelain-restored teeth in the mass dental examinations

In the mass dental health examinations, the evaluation of accurate oral health status is useful not only for the planning of oral health and welfare programs but also for the appropriate oral health guidance and care of individuals. These evaluations would greatly contribute to the progress of Quality of Life for people from the viewpoint of preventive dentistry. The procedure to make porcelain restorations requires much more time and labor which results in much more prominent aesthetics compared with other esthetic materials like composite resin. Thus, it is very difficult to detect the teeth restored with porcelain. To obtain more reliable survey results, we need a more accurate detection method for porcelain-restored teeth.

4.2 Excitation spectra

To examine the difference of fluorescence properties between porcelain and tooth, the excitation spectra was measured for the fluorescence at the wavelength of 500 nm. The broad wavelength was observed in the full width of half maximum (FWHM) for the fluorescence at 500 nm (Fig. 2), and there was a clear difference in the fluorescence intensity with an excitation light over 400 nm. This suggested that the fluorescence emission of tooth was brighter than all the porcelains at excitation light longer than 400 nm. Fluorescence spectra of tooth obtained from six teeth showed that the individual difference is small for peak wavelength, intensity and width, especially in the longer wavelength side. These suggest that the discrimination of porcelain from tooth was possible using the fluorescent properties.

4.3 Dependence of fluorescence on shade difference

Various colors are supplied for porcelain to correspond with teeth so that restoration is not conspicuous. Therefore,

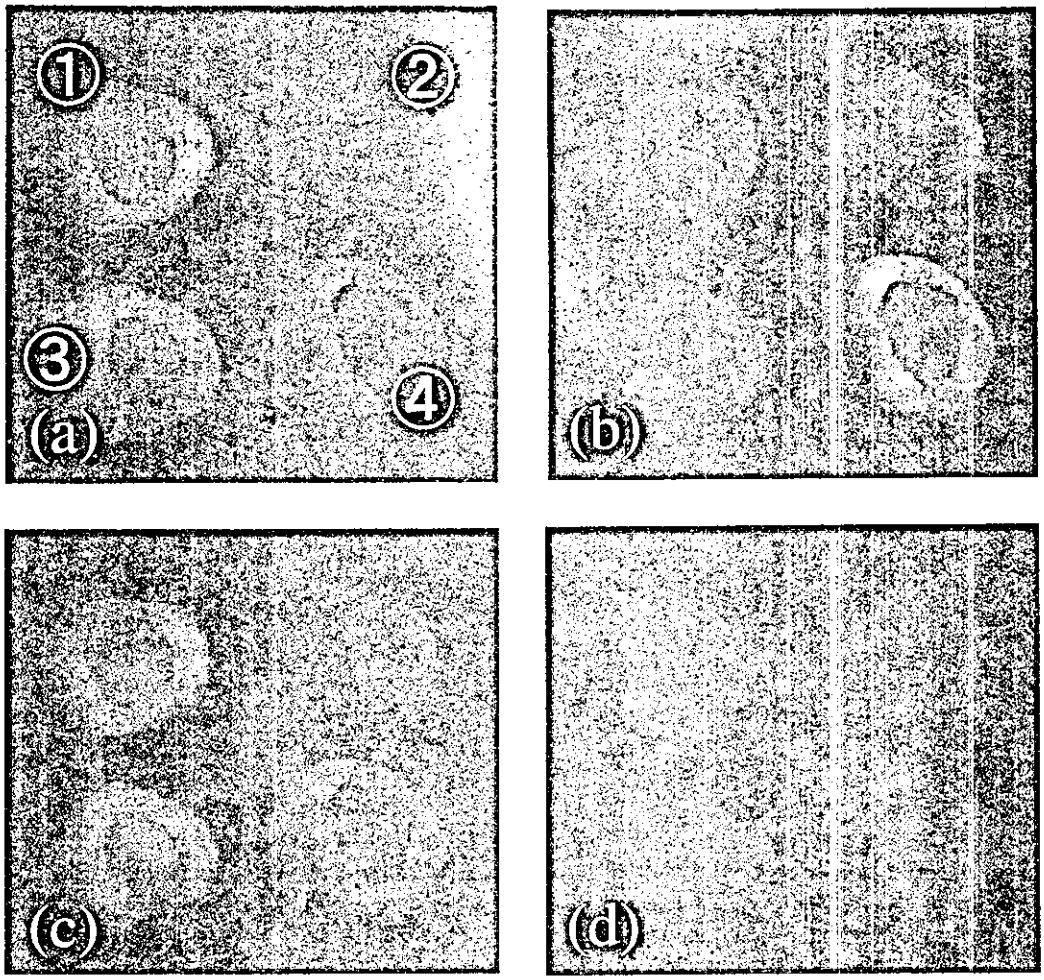

Fig. 7 Fluorescence image of the porcelain-restored tooth with different excitation lights 40(a), 43(b), 45(c), L47(d).

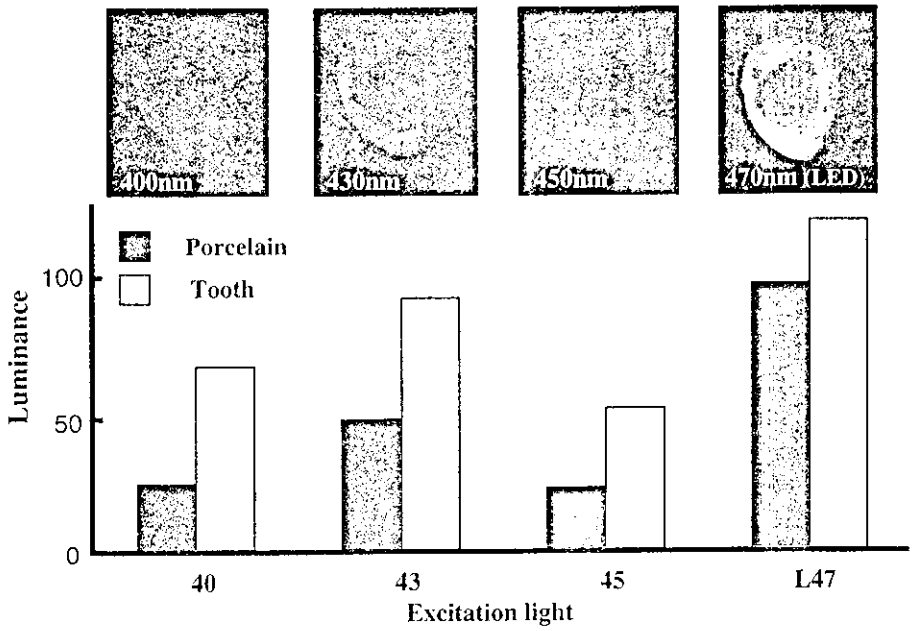

Fig. 8 Fluorescence image (>500 nm) of the porcelain-restored tooth with excitation lights 40, 43, 45, L47, and the corresponding luminance of porcelain and tooth.

the fluorescence spectra were studied for each shade. As shown in Fig. 3, the fluorescence spectra were similar with nearly the same peak position and similar intensity. Therefore, one could conclude that the shade of porcelains does not practically affect the fluorescent properties.

4.4 The optimum discrimination condition

Fluorescence spectra of each A3 shade porcelain and tooth were compared for the 380, 400, 430, 450 and 470 nm excitation wavelengths. The fluorescence of tooth is stronger than all the porcelains at excitation light, over 400 nm, as shown in the excitation spectra of tooth and porcelain (Fig. 2). In the fluorescence spectra excited by 380 nm wavelength, fluorescence intensities of each enamel porcelain were similar to tooth. For the 400, 430, 470 nm excitation, the fluorescence intensity of tooth was stronger than all the porcelains of both enamel and dentin in the range longer than 500 nm. Under these conditions, discrimination is possible.

4.5 Fluorescence image

To examine if the discrimination is visually feasible, the fluorescence image of porcelain-restored tooth was photographed under the conditions suggested from spectroscopy. For the excitation light 40, 43, 45 and L47, the tooth part of the porcelain-restored tooth was brighter and discrimination was possible in correspondence with the fluorescence spectra of Fig. 5 and Fig. 6. The degree of difference was also quantitatively evaluated by comparing the luminance of porcelain and tooth. Fig. 8 showed that tooth emitted the strongest fluorescence by excitation light L47 with the blue LED. This may be because the LED produced the strongest light intensity compared to that of excitation lights 40, 43 and 45 (Fig. 1). Regarding the luminance ratio of tooth to porcelain, the excitation light 40 provided the highest as shown in Fig. 8. This is in agreement with the fact that the difference of fluorescence emission between tooth and porcelain was larger than others as shown in the spectra by the 400~470 nm excitations (Fig. 5, 6).

4.6 The possibility on clinical application

Discrimination of tooth from aesthetic materials close, in luster and shades, to natural tooth was difficult in mass dental examinations. The present detection methods of teeth restored with aesthetic materials using visual inspection or palpation with explorers have not been very accurate detection methods, and take a long time. Furthermore, palpation using explorers with sharp tips carry the risk of tooth damage. If accurate, easy and non-contact visual detection methods with reproducibility were made possible, efficient examination without the early incidence of caries by exploring could be carried out. This fluorescence study found that the suitable range of excitation light for discrimination is 400~450 nm in order to give a good luminance contrast. The previous study for composite resin showed that excitation light 430~460 nm provided a good luminance contrast. Therefore the excitation light of wavelengths ranging from 430 to 450 nm would satisfy the discrimination in the cases of both composite resin and porcelain. The observation of fluorescence image was obtained only in a dark environment in these studies. A stronger light source is necessary for use in a bright place, since fluorescence emission is in proportion to the intensity of excitation light. As an excitation light source, LED seems suitable for clinical application because of its high emission intensity, and convenience because a filter is not necessary.[12] Long life and small electricity consumption are also appropriate as a light source for mass dental health examinations. However, as a light source for differentiation, it is not currently optimal since the peak wavelength of a marketable LED is 470 nm. The detection ability may be increased with the improvement of higher intensity and suitable wavelengths for LED's in the future. In addition, the amplifying system of fluorescence image is desirable to enhance the visual detection ability of teeth restored with aesthetic material.

5. Conclusions

As a basic research for the visual detection of porcelain-restored teeth in mass dental health examinations, the discrimination of porcelain from tooth was examined using the fluorescent properties, and the following findings were obtained.

(1) Fluorescence difference by color shade of porcelain is small at 400 nm excitation.
(2) Fluorescence of tooth is stronger than porcelain by excitation with wavelengths over 400 nm.
(3) The optimum condition (430~450 nm) for discrimination of tooth from porcelain in the fluorescence image is in agreement with the condition suggested by the fluorescence spectra.
(4) As an excitation light source, the high brightness and operability provided by LED is more suitable.
(5) The fluorescence difference can successfully discriminate the porcelain from tooth and recognize the restored tooth, which suggests the possibility of a non-contact detection method in mass dental health examinations without having to use the exploring method.

REFERENCES

1) L. S. Turkun, B. O. Aktener and M. Ates: Quintessence. Int. **34** (2003) 418–426.
2) J. W. van. Dijken: J. Dent. **28** (2000) 299–306.
3) G. J. Christensen: J. Am. Dent. Assoc. **126** (1995) 1427–1428.
4) K. H. Chung: J. Dent. Res. **69** (1990) 852–856.
5) D. Dietschi and J. Holz: Quintessence. Int. **21** (1990) 965–975.
6) M. Hayashi, Y. Tsuchitani and M. Miura: Oper. Dent. **23** (1998) 318–326.
7) A. Scheibenbogen, J. Manhart and K. H. Kunzelmann: J. Prosthet.Dent. **80** (1998) 410–416.
8) A. J. Qualtrough and N. H. Wilson: J. DENT. **24** (1996) 317–23.
9) F. Isidor and K. Brondum: J. Prosthet. Dent. **74** (1995) 140–144.
10) R. E. Jordan and M. Suzuki: J. Estet. Dent. **1** (1989) 41–44.
11) K. Tani, F. Watari, M. Uo and M. Morita: Dent. Mater. J. **22** (2003) 569–580.
12) S. Nakamura, M. Senoh, N. Iwasa and S. Nagahana: Appl. Phys. Lett. **67** (1995) 1868–1870.

Materials Transactions, Vol. 45, No. 4 (2004) pp. 1033 to 1040
Special Issue on Frontiers of Smart Biomaterials

EXPRESS REGULAR ARTICLE

Non-Contact Surface Morphology Analysis of CO_2 Laser-Irradiated Teeth by Scanning Electron Microscope and Confocal Laser Scanning Microscope

Magda Kiyoko Yamada*, Motohiro Uo, Shoji Ohkawa, Tsukasa Akasaka and Fumio Watari

Division of Dental Materials and Engineering, Department of Oral Health Science, Graduate School of Dental Medicine, Hokkaido University, Sapporo 060-8586, Japan

A newly developed scanning electron microscope (SEM) installed with a 3D analyzer and a confocal laser scanning microscope (CLSM) were used to evaluate the images and surface profiles of enamel and dentin after CO_2 laser irradiation. The surface roughness (*Ra*) was measured and the results were correlated with a stylus profilometer. Raman analysis was done and the laser irradiation effect after acid etching was also examined. Human intact extracted teeth were vertically sectioned. The laser was applied perpendicularly to non-etched and 35% phosphoric acid-etched teeth. The enamel resulted in a crater-like surface. The material was removed in the places where hydroxyapatite crystallites ran parallel to the irradiated surface. Non-etched dentin showed little change after irradiation, with some cracks mostly in the peritubular dentin; whereas in acid-etched dentin there was evaporation of collagen and melting of hydroxyapatite. The SEM and CLSM showed similar profiles and different image contrast. *Ra* levels obtained by the SEM and CLSM were similar to that obtained with the stylus profilometer. Raman analysis showed that bands of organic collagen matrix on dentin were lost and broad peaks due to carbon were observed. Both the SEM and CLSM provided non-contact evaluation of structural changes of teeth by laser irradiation through surface analysis in selected microareas, which was not possible using the stylus profilometer. Dentin showed more structural changes on the acid-etched surface by irradiation than on the non-etched one.

(Received November 7, 2003; Accepted February 2, 2004)

Keywords: *scanning electron microscope (SEM), confocal laser scanning microscope (CLSM), tooth, acid etching, CO_2 laser*

1. Introduction

The irradiation effect of the CO_2 laser on teeth has been studied from the aspect of surface morphology. CO_2 laser irradiation of the enamel and dentin surface was reported to cause surface fusion.[1] The characterization of the enamel surface changes according to the wavelength dependence, as revealed by surface melting, crystal fusion and exfoliation.[2] Watari analyzed the effect of CO_2 laser irradiation for the same spot on human teeth by employing three different microscopes, a scanning electron microscope (SEM), confocal laser scanning microscope (CLSM) and atomic force microscope.[3] However, the quantitative analysis of surface morphology has been limited. A conventional stylus profilometer has usually been used to measure roughness, but the measurements are separate from SEM imaging. The surface roughness (*Ra*) value measured by a single device does not necessarily offer a comprehensive picture of the surface.[4] It was reported that the contact stylus profilometer gives a lower *Ra* than an optical profilometer due to the limitations of the stylus dimensions of the stylus in detecting microgrooves.[5] Furthermore, the stylus profilometer can cause damage to the dental hard tissue due to the contact with the specimen.

The newly developed three-dimensional (3D) analyzing SEM and CLSM can provide imaging and non-contact profile analyses simultaneously in a selected microarea with high spatial resolution. The CLSM has the advantage of being a non-destructive method since sample preparation is not necessary, and it also allows subsurface analysis.[6] SEM has higher resolution and analysis without coating is also possible if a low acceleration voltage is used. Until now, however, only the imaging results have been observed. Recently, a SEM with a 3D-analyzer has been developed using reflection electrons with 4-quadrant divided detectors to make possible quantitative surface analysis.

Chemical analysis of the laser-irradiated surface is also important. From this aspect, Raman spectroscopy can give information about the chemical state without damage.[7] Another advantage is that the spatial resolution of about 1 micrometer (μm) allows chemical and structural information to be obtained within the μm range.

This study simultaneously combined imaging and non-profile analyses of surface morphology using the SEM and CLSM, and added compositional information obtained by Raman spectroscopy to evaluate the effects of the CO_2 laser on the enamel and dentin surfaces. The data obtained using the SEM and CLSM from the same area of the specimen were also correlated with the conventional stylus profilometer. Further microscopic observation was done to evaluate the additional effect of acid-etching pretreatment before laser irradiation by analyzing the results for non-etched and acid-etched dentin.

2. Materials and Methods

2.1 Specimen preparation

Five freshly extracted, intact, caries-free human third molars and pre-molars were used in this study. They were cleaned and stored in deionized water at 4°C until used. Vertical sectioning parallel to the long axis of each tooth was done using a low-speed diamond saw (Minitom, Struers, Copenhagen, Denmark) under running water. Two slabs from each tooth with thicknesses of 2 mm were obtained. The exposed enamel and dentin of both slabs were polished with alumina powder (2 μm, 1 μm and 0.05 μm successively), rinsed and ultrasonicated in deionized water to remove the polished debris. One slab of each tooth was kept wet in

*Graduate Student, Hokkaido University

deionized water until the application of the laser. The other was immersed in 35% phosphoric acid for 5 minutes to expose the collagen fibrils prior to the laser treatment.

2.2 Laser irradiation

The laser apparatus used was a CO_2 laser (Model Panalas C10, Panasonic, Osaka, Japan) with a wavelength of 10.6 μm. It was set with a pulse duration time of 0.5 s with a 2 mm diameter tip and work distance of approximately 1 mm. A single pulse irradiation with 3–8 W of power was done perpendicularly to enamel and dentin.

2.3 Observation and surface analysis

2.3.1 Digital microscope

Digital Microscope (VH-6300, Keyence Corporation, Osaka, Japan) was used and the specimen was observed at ×25 magnification.

2.3.2 SEM

The specimens were analyzed using SEMs (S-4700 and S-4000, Hitachi, Tokyo, Japan). A 3D analyzer (RD-500W) installed in the SEM S-4700 (3D-SEM) was used for 3D and depth profile analysis. The S-4700 operates using a cold field emission electron source and has high resolution at low acceleration voltage. The device provides secondary electron (SE) and backscattered electron (BSE) images. The specimens were observed at an acceleration voltage of 3 kV and no sputter coating was done to allow the same specimen to be examined by other microscopes. Specimens treated with phosphoric acid were carbon coated and observed using the SEM S-4000 under acceleration voltages of 5 kV and 10 kV.

2.3.3 Confocal laser scanning microscope (CLSM)

The same specimen examined using the SEM S-4700 was observed by CLSM (LSM 410 Invert, Carl Zeiss, Oberkochen, Germany) in the reflection mode through a 543 nm He-Ne laser, with an objective lens of 50× and a numerical aperture of 0.85. A series of optical sections parallel to the tooth surface was obtained from each specimen. The pinhole was set to 10, which gave a full width at half maximum (FWHM) peak of 1.33 μm. The distance between sections was 0.5 μm. All data were documented at a resolution of 768 × 576 pixels. The surface topography software allows surface roughness analysis of the tooth as well as 3D reconstruction of the images from section series. The surface profile and roughness analyzed using the SEM and CLSM were then compared.

2.3.4 Stylus profilometer

The surface roughness was analyzed using a conventional stylus profilometer (Surfcom 200C, Tokyo Seimitsu, Tokyo, Japan). The vertical magnification was adjusted to 500 K, chart speed 3 mm/s and tracing speed 0.03 mm/s. The *Ra* values were determined as the average height deviation, in μm, from the mean plane through widths of 800 μm and 250 μm for both enamel and dentin.

2.3.5 Raman spectroscopy

Raman spectra of non-irradiated and laser-irradiated surfaces were obtained using a Raman spectrometer (Labram, Horiba, Tokyo, Japan). Specimens were excited with a He-Ne laser (632.8 nm) at 40 mW through a microscope objective lens (100×, NA = 0.90). The focal spot size was about 1 μm in diameter. The spectra were recorded at a resolution of 2 cm^{-1}.

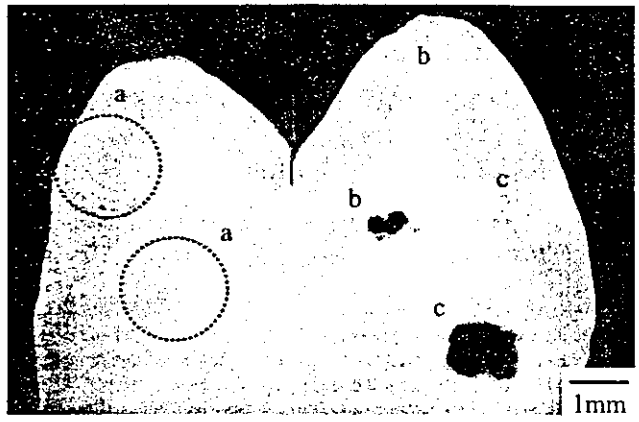

Fig. 1 Vertical section of tooth irradiated by CO_2 laser. a, b and c indicated in enamel and dentin were irradiated at 3 W, 6 W and 8 W, respectively.

3. Results

Figure 1 shows a digital microscope image of a vertically sectioned tooth irradiated by the CO_2 laser. Therein, a, b and c indicate that the enamel and dentin were irradiated at 3 W, 6 W and 8 W, respectively. The size of lased-area increased with the power. Enamel became white and dentin black due to carbonization of collagen.

Figure 2 shows the SEM images and respective depth profiles of enamel and dentin irradiated at 6 W. The surfaces irradiated at 6 W were the most representative, and were therefore chosen for the analysis. The profiles were obtained in a non-contact mode along the horizontal line in the SEM micrographs. Enamel showed a crater-like surface, while dentin had a very smooth surface. Both had cracks due to the thermal shock. The laser-irradiated area became light white compared to the surrounding non-irradiated area. The *Ra* was 5.12 μm for enamel and 1.09 μm for dentin. The square areas delimited in SEM micrographs of enamel and dentin were enlarged and compared with those of the CLSM in Figs. 3 and 4, respectively.

Figure 3 shows the SEM and CLSM images and their respective profiles from the identical area of laser-irradiated enamel. The bright contrast observed at the edges of the grooves in SEM image became dark in CLSM. The depth profiles obtained in the non-contact mode showed similar outlines. The formation of grooves resulted in *Ra* of 3.17 μm for SEM and 6.17 μm for CLSM analysis.

Figure 4 shows a comparison of SEM and CLSM images and their respective profiles of laser-irradiated dentin. With the SEM, dentinal tubules and cracks were observed. However, with the CLSM the interior of dentinal tubules was also observed, differentiating them from the cracks. The depth-profile analysis from both the SEM and CLSM showed roughness of 0.12 μm for SEM and 0.78 μm for CLSM.

Conventional stylus profilometer analysis was also done. The profile was detected by a stylus profilometer that passed 800 μm and 250 μm from nearly the same area as in Fig. 2. The *Ra* values measured along 800 μm were 3.63 μm for enamel and 0.39 μm for dentin. At 250 μm, *Ra* was 2.35 μm

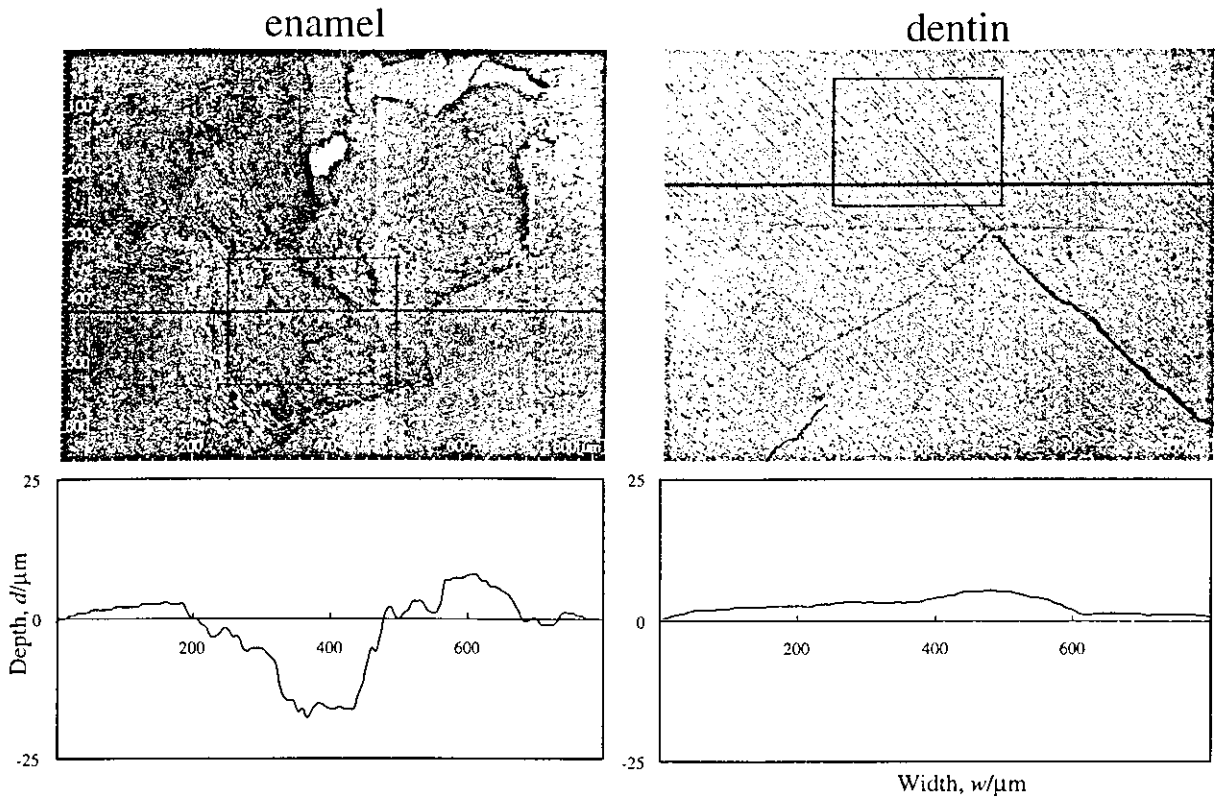

Fig. 2 SEM images and respective depth profiles obtained from the irradiated area of enamel and dentin at 6 W. The profiles were obtained in a non-contact mode along the horizontal line in the SEM micrographs. The enclosed areas are enlarged and compared with those from the CLSM in Figs. 3 and 4.

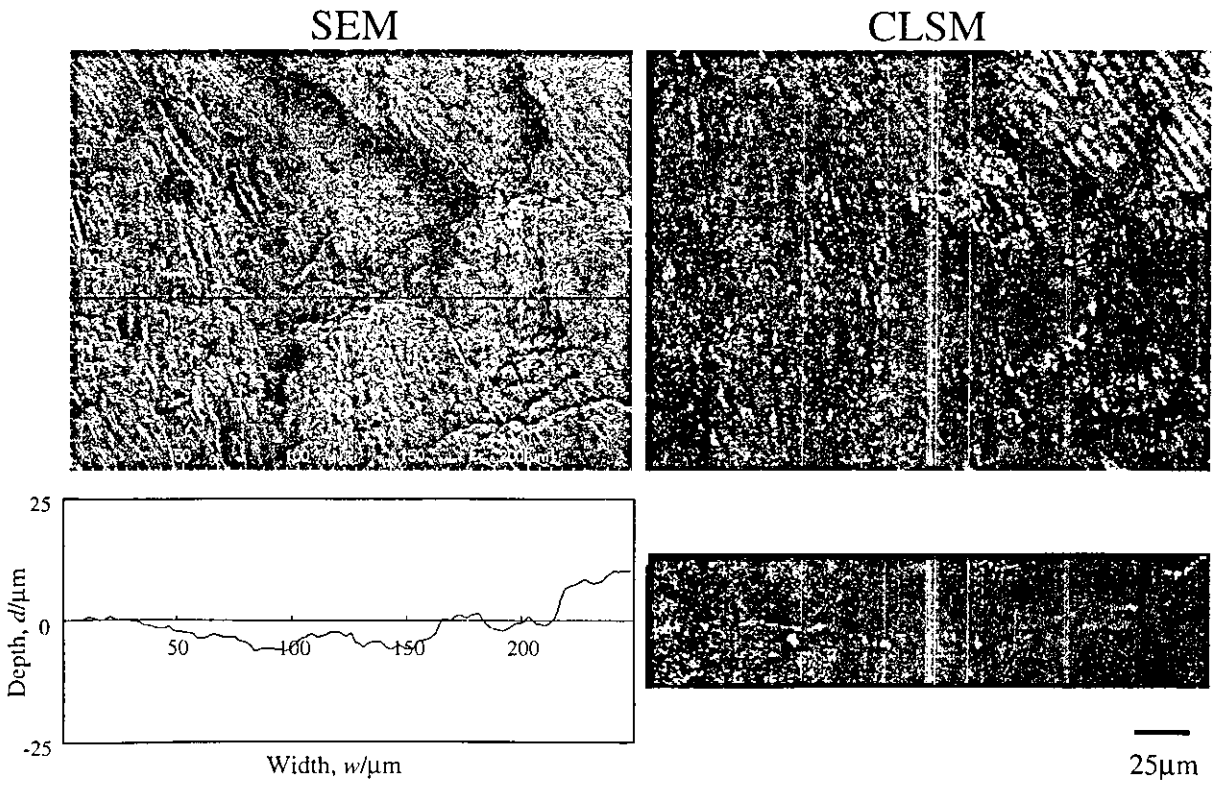

Fig. 3 SEM and CLSM images and their respective profiles of laser-irradiated enamel obtained from the same area of the same specimen. The images are enlargements of the areas delimited in Fig. 2.